PHYSICAL REVIEW B VOLUME 21, NUMBER 6 15 MARCH 1980

# Laser-induced line-narrowing of $Eu^{3+}$ fluorescence in fluoroberyllate glass: Site-dependent spectroscopic properties and their structural implications

C. Brecher and L. A. Riseberg
*GTE Laboratories, Inc., Waltham, Massachusetts 02154*
(Received 9 July 1979)

The techniques of laser-induced fluorescence line-narrowing were applied to the study of the spectroscopy of $Eu^{3+}$ in a KCaAl fluoroberyllate glass. Large systematic changes were observed in the intensities and wavelengths of the various features of the emission and in the decay times of that emission. Using previously developed criteria, the site-dependent behavior of the $^5D_{0,1}$ states and of all Stark components of the $^7F_{0,1,2}$ states were derived; calculations using the electrostatic crystal-field approach were performed and gave a good fit to the observed splittings across the entire range of sites. The structural model derived for oxide glasses was found to be inadequate to explain the observed behavior, but an acceptable alternate model was derived; this model involves a ninefold coordination of $Eu^{3+}$ by two sets of nonequidistant fluoride ions and a systematic axial distortion of this arrangement.

## I. INTRODUCTION

With the advent of laser-induced fluorescence line narrowing, it has now become possible to probe spectroscopically various details of the microstructure of glassy systems. Following the first demonstrations of the line-narrowing phenomenon,[1,2] various investigations have revealed site-dependent details of interionic energy-transfer processes,[3,4] homogeneous linewidths,[5,6] radiative and nonradiative transition probabilities,[7-10] and local coordination structure.[11-13] In the last named area, we established that the line-narrowed emission spectra of the $Eu^{3+}$ ion in silicate glass[11] was consistent with a distribution of sites involving a gradual and continuous change from largely eightfold to largely ninefold coordination. Subsequent work[12-15] also revealed that the same model was applicable to glasses consisting of a wide range of tetrahedral oxidic network formers (silicates, phosphates, borates, aluminates, and combinations), with the differences being essentially matters of detail. In the present work, we report a comprehensive spectroscopic study of a fluoroberyllate glass doped with $Eu^{3+}$. We find that, despite its nominally similar glassy network, this nonoxidic glass former gives rise to a totally different pattern of behavior, and requires a new coordination model to explain the observations.

## II. EXPERIMENTAL

Although many glasses can be made which contain fluorides as major constituents, most such systems require at least a small proportion of oxidic components to stabilize the glassy network. Among the few known stable, fully fluoride (oxide-free) glasses,[16] the most noteworthy is the fluoroberyllate; while other systems, particularly the fluorozirconate,[17-19] have been examined to various degrees, only the fluoroberyllate, with its network of tetrahedral $BeF_4$ groups, can come close to serving as a fluoridic analog to most of the common oxidic glasses. The particular material chosen for this investigation was a KCaAl fluoroberyllate, with the following nominal composition in mole percent: $BeF_2$, 48; KF, 27; $CaF_2$, 14; $AlF_3$, 10; and $EuF_3$, 1. The specimen was an optically clear and homogeneous rectangular prism with polished faces, about 3 mm × 3 mm in cross section and about 12 mm long, and was maintained in an optical cryostat at a temperature of about 80 K.

Line-narrowed fluorescence from the specimen was excited by means of a tunable pulsed dye laser, consisting of an ethanolic dye solution circulated through a cylindrical cell with wedged windows and excited transversely by an Avco C950 pulsed nitrogen laser at a rate of about 20 Hz. The dye laser pulses were about 15 nsec in duration with a spectral width <0.1 nm, unpolarized, and their wavelength was tuned by an intracavity grating. The resultant emission, also unpolarized, was measured with a Jarrell-Ash 1-m Czerny-Turner monochromator and a Varian VPM-159S flat response photomultiplier, and time-resolved integration of the fluorescence signal was provided by a PAR Model 160 Boxcar Integrator. The complete apparatus is depicted in Ref. 11. Spectra were measured in the range from 570–640 nm, corresponding to emission from the $^5D_0$ to the $^7F_{0,1,2}$ levels and between 520 and 570 nm, corresponding to emission from the $^5D_1$ to the same lower levels. Line-narrowed emissions corresponding to the $^5D_0 \rightarrow {}^7F_{3,4}$ transitions were also measured, but did not prove useful. Measurements were also made of the fluorescence under

broad-band UV excitation (Fig. 1), using a repetitively pulsed xenon flash lamp, and of the resonant absorption to the $^5D_{0,1,2}$ states (Fig. 2), using a chopped dc tungsten light source.

Line-narrowed fluorescence is generated by the excitation, within the inhomogeneously broadened absorption envelope of a single transition, of a given subset of sites (called an isochromat[20]) whose homogeneous absorption exactly coincides with the wavelength of the incident radiation. Equivalent isochromats, with almost identical emissions, can be excited through different transitions, usually at about the same relative positions in the respective inhomogeneous envelopes. If such envelopes overlap, inequivalent isochromats can absorb at the same absolute wavelength, each making its own different contribution to the total emission. To eliminate such spectral ambiguity, it is highly desirable that excitation be accomplished through a spectrally isolated absorption, not split by the crystal field. In the various oxidic glass systems previously studied, the $^7F_0 \rightarrow {}^5D_0$ transition was ideally suited for such excitation; in the case of the fluoroberyllate, however, this absorption proved far too weak, even at $Eu^{3+}$ concentrations as high as 5 mole percent. This weakness is a manifestation of the general reduction of electric dipole transition strengths in this material, also reflected by the unusually long fluorescence decay time (≈10 msec). These points will be discussed later.

It did prove feasible to utilize the absorption to the $^5D_1$ and $^5D_2$ states (Fig. 2) to obtain line-narrowed fluorescence. However, unlike the $^5D_0$, which cannot be split by the crystal field at the site, these two higher states are split into three and five Stark components, respectively, and the inhomogeneously broadened envelopes of the individual components overlap considerably. Only by limiting our excitation range to the short- and long-wavelength wings of the respective absorption regions could we selectively excite relatively pure isochromats, unclouded by extraneous contributions. In this case, it is the emission from the $^5D_0$ to the $^7F_0$ that is used to characterize the site-selection process, with its wavelength used as an identifying index and its width and spectral purity (absence of multiple peaks) as a criterion of site selectivity. Excellent correlation between line-narrowed spectra excited directly into the $^5D_0$ and those obtained from the higher states has already been demonstrated in a borate glass,[21] although the site selectivity achieved in those measurements under pumping into the $^5D_1$ was far from complete. In the case of the fluoroberyllate, however, excellent site selectivity was achieved by pumping into both long- and short-wavelength wings of the absorptions into either the $^5D_1$ or $^5D_2$ states. Furthermore, in this glass it proved possible to move the excitation wavelength a sufficient distance toward the center of the absorption, before degradation of site selectivity became intolerable, to span the entire range of $^5D_0 \rightarrow {}^7F_0$ energies. This fact, and the absence of any significant discontinuity in spectral behavior, would indicate that the set of line-narrowed spectra obtained in this work is at least as complete as in the previously reported work on silicate glass.[11]

Excitation into the $^5D_1$ and $^5D_2$ states requires dye lasers other than the Rhodamine 6G used earlier. In the green spectral region corresponding to the $^7F_0 \rightarrow {}^5D_1$ absorption, a mixed ethanol solution

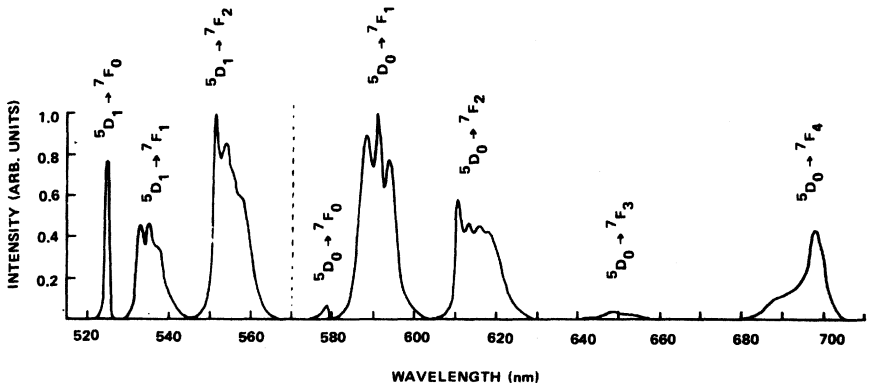


FIG. 1. Fluorescence emission from $Eu^{3+}$ in KCaAl fluoroberyllate glass (at 80 K) when excited by pulsed broad-band ultraviolet. Delay after excitation, 100 μsec for $^5D_1$ emission, 1 msec for $^5D_0$ emission. Intensities of $^5D_1$ emission normalized relative to most intense $^5D_1 \rightarrow {}^7F_2$ peak; intensities of $^5D_0$ emission normalized relative to most intense $^5D_0 \rightarrow {}^7F_1$ peak. Note dominance of magnetic dipole ($^5D_1 \rightarrow {}^7F_{0,2}$ and $^5D_0 \rightarrow {}^7F_1$) transitions and generally similar spectral structure in emissions terminating in same $^7F$ multiplet.

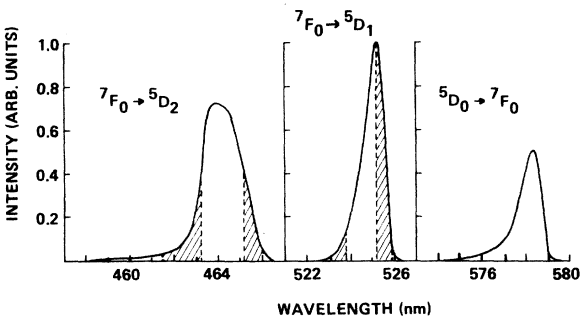


FIG. 2. Inhomogeneously broadened profiles of transitions between $^7F_0$ and $^5D_{0,1,2}$ states. The $^7F_0 \rightarrow {}^5D_{1,2}$ transitions are measured in absorption, in terms of $-\ln I/I_0$, and are directly comparable in intensity; shaded areas denote wavelengths where laser excitation yielded relatively pure isochromats. The $^5D_0 \rightarrow {}^7F_0$ transition is measured in emission, with indicated limits showing range of wavelengths over which line-narrowed emission, characteristic of individual isochromats, was measured.

of Coumarins 7 and 120 was used, the latter to enhance the response of the dye at the wavelength of the $N_2$ laser. Line-narrowed emission from the $^5D_0$ state was measured at excitation wavelengths between 522.6 and 5.25.8 nm at 0.2-nm intervals. The gated detection window was set at 100 $\mu$sec in width, centered at a 1 msec delay after the excitation pulse. Although longer than in previous work, this delay was only about 10–15% of the measured decay time of the $^5D_0$ state and was selected only after measurements at shorter delays, down to 100 $\mu$sec, had revealed no noticeable deterioration in the line-narrowing effect, and hence no significant site-to-site energy migration over this time span. The difficulty with measurements at the shorter delay times is that the decay of the $^5D_1$ state is also unusually long (in the 200-$\mu$sec range), presumably because of the decreased multiphonon decay rates in fluoride hosts,[22] with a correspondingly long rise time of the $^5D_0$ emission. Thus measurements at a 1-msec delay were necessary to minimize distortion of the $^5D_0$ spectra by extraneous contributions from the $^5D_1$ state in regions where emissions from the two states overlap.

For excitation in the blue region of the spectrum, corresponding to the $^7F_0 \rightarrow {}^5D_2$ absorption, a solution of Coumarin 2 in ethanol proved satisfactory. Line-narrowed emission spectra were recorded at excitation wavelengths between 460 and 466 nm, generally at 0.2-nm intervals. The emission from the $^5D_0$ state was recorded under the same conditions as described earlier for excitation into the $^5D_1$ state; in addition, however, the emission from the $^5D_1$ state was also measured, with a 10-$\mu$sec window centered at 100 $\mu$sec after the excitation flash. These measurements were generally restricted to wavelengths shorter than 570 nm, corresponding to emissions from the $^5D_1$ to the $^7F_{0,1,2}$ states. Emissions from the $^5D_1$ at wavelengths longer than 570 nm were recorded for completeness, but were not spectroscopically useful because of the overlap with those from the $^5D_0$.

At most of the excitation wavelengths, the time profile of the decay of the line-narrowed fluorescence from the $^5D_0$ state was also measured. To maximize spectral discrimination, the monochromator was set at the wavelength of the sharpest and spectrally purest emission line of the spectrum, namely, the $^5D_0 \rightarrow {}^7F_0$ emission characteristic of the particular isochromat selected by the excitation pulse. Because of the relative weakness of this transition, however, signal-averaging techniques (utilizing a Nicolet Model 1073 Signal Averager) were necessary, and it sometimes required as much as thirty minutes to extract a reasonably noise-free waveform. Similar measurements were also made on the non-line-narrowed emission under broad-band excitation; this decay deviated only slightly from the functional form of a single exponential, reflecting a preponderance of long-lifetime sites in the glass. Under line-narrowing conditions the decays were strictly exponential.

## III. RESULTS

The spectroscopic measurements under line-narrowing conditions are shown in Fig. 3. The left-hand portion displays a series of selected line-narrowed emission spectra of the $^5D_0 \rightarrow {}^7F_{0,1,2}$ transitions obtained by excitation at various wavelengths in the inhomogeneously broadened $^7F_0 \rightarrow {}^5D_1$ absorption, as well as a non-line-narrowed spectrum obtained by broad-band excitation in the ultraviolet. The right-hand portion shows a similar, more extensive series obtained by excitation into the $^5D_2$ state. All the possible Stark components of these emissions (one, three, and five, respectively), are measurable, although some are partially obscured by their neighbors. The $^5D_0 \rightarrow {}^7F_{3,4}$ emissions, however, are not only incompletely resolved, but also show virtually no excitation-dependent spectral changes (Fig. 4), and hence are not useful in the subsequent discussions.

The line-narrowed spectra obtained through either $^5D_1$ or $^5D_2$ excitation are indexed by the wavelengths of their $^5D_0 \rightarrow {}^7F_0$ emission, and a unique correspondence can be made between spectra obtained by pumping into the two different upper states; specifically, each measured wavelength for the line-narrowed $^5D_0 \rightarrow {}^7F_0$ emission

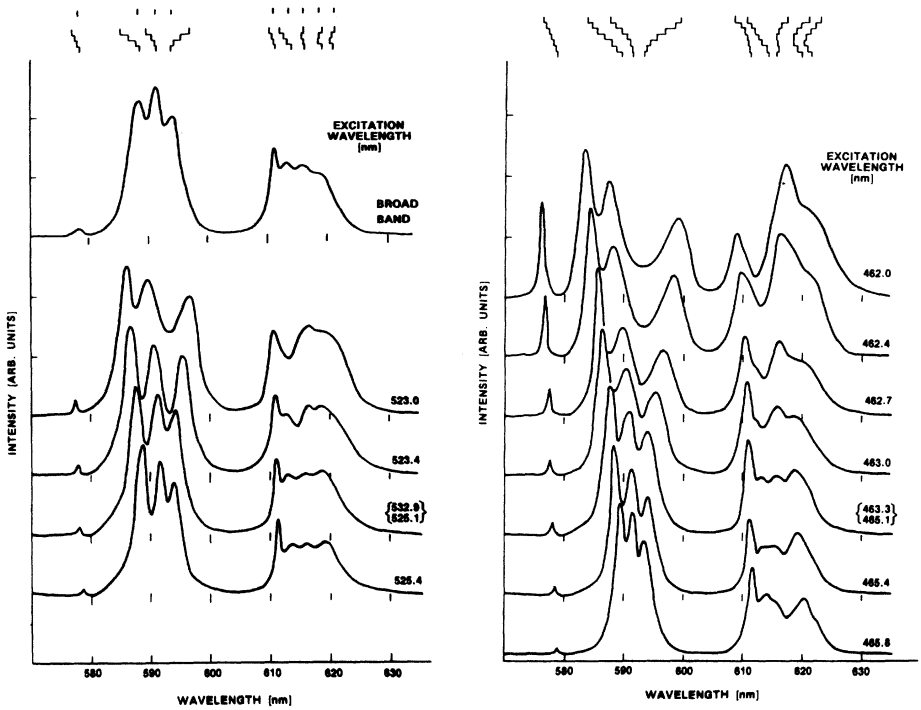


FIG. 3. Line-narrowed fluorescence emission from the $^5D_0 \rightarrow {}^7F_{0,1,2}$ transitions of $Eu^{3+}$ in KCaAl fluoroberyllate glass (at 80 K) as function of excitation wavelength. Delay after excitation, 1 msec. Intensities normalized to most intense $^5D_0 \rightarrow {}^7F_1$ peak. Tick marks at top of figure show wavelength shifts of the respective emission peaks as functions of excitation. The spectra obtained when pumped into the $^5D_1$ manifold (left) and the $^5D_2$ manifold (right) are displayed so that those on the same horizontal line come from equivalent isochromats; that is, they correspond in the wavelengths of all nine spectral components In the $^5D_2$ set, the three spectra at the lowest-excitation wavelengths had been underlain by a broad-band background, which was subtracted out in these figures to clarify the features of the line-narrowed spectra (see text). The background was essentially identical to the spectrum obtained under broad-band ultraviolet excitation, shown (upper left) at the same scale for comparison.

has associated with it one and only one set of $^7F_1$ and $^7F_2$ energies. Despite some differences in relative intensity, the correspondence is quite good (generally within 3 $cm^{-1}$), indicating that

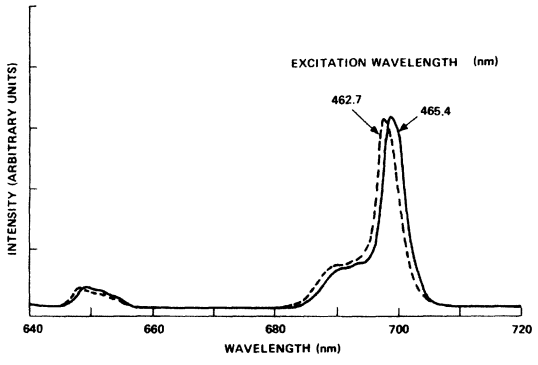


FIG. 4. Fluorescence emission from the $^5D_0 \rightarrow {}^7F_{3,4}$ transitions at two excitation wavelengths. For comparison with Fig. 3, divide these intensities by two; other conditions as before. Note poorly resolved features and insignificant excitation dependence.

equivalent isochromats, characteristic of environments with nearly identical crystal-field splittings, can be selected independently of the choice of pumping levels.

As for intensities, however, the situation is somewhat more complex. One immediately evident feature is the dominance of the $^5D_0 \rightarrow {}^7F_1$ magnetic dipole transition. The hypersensitive $^5D_0 \rightarrow {}^7F_2$ electric dipole transition, normally the dominant emission from $Eu^{3+}$ in oxidic glasses, is severely suppressed, as are the $^5D_0 \rightarrow {}^7F_0$ and $^5D_0 \rightarrow {}^7F_4$ to a somewhat lesser degree. This behavior strongly resembles that of $Eu^{3+}$ in a centrosymmetric site,[23] and is a manifestation of the anomalously low Judd-Ofelt intensity parameter $\Omega_2$, characteristic of most rare-earth fluoride systems.[24] This effect is felt in the transitions from the $^5D_1$ state as well, but with the opposite sense; inasmuch as the $^5D_1 \rightarrow {}^7F_0$ and $^5D_1 \rightarrow {}^7F_2$ are magnetic dipole transitions, it is they that are dominant over the electric dipole type $^5D_1 \rightarrow {}^7F_1$. The complementary nature of the $^5D_0$ and $^5D_1$ emissions and the corresponding differences in selec-

tion rules prove quite useful in making spectroscopic assignments, discussed later.

Despite their general similarity, the spectra obtained by excitation into the two different upper states do show noticeable differences in intensity distribution. The most important of thise is that pumping into the electric dipole type $^7F_0 \rightarrow {}^5D_2$ absorption yields line-narrowed spectra with a relatively greater proportion of electric-dipole-type emission ($^5D_0 \rightarrow {}^7F_{0,2}$), while pumping into the magnetic-dipole-type $^7F_0 \rightarrow {}^5D_1$ absorption yields relatively more magnetic dipole $^5D_0 - {}^7F_1$ emission. The same kind of change in the branching ratio, although somewhat smaller, can be observed even under broad-band excitation, if this excitation is spectrally limited to the regions of the $^7F_0 \rightarrow {}^5D_1$ or $^7F_0 \rightarrow {}^5D_2$ absorption, respectively. Furthermore, the inhomogeneous breadth of the $^7F_0 \rightarrow {}^5D_2$ absorption appears considerably greater than that of the $^7F_0 \rightarrow {}^5D_1$ (or the wings more intense), making it possible to obtain line-narrowed emission over a wider range of sites. Indeed, those sites having the highest electric dipole transition probabilities (and readily identified by the anomalously high intensity of their $^5D_0 \rightarrow {}^7F_0$ emission), are accessible to observation only by excitation into the $^5D_2$ state.

The variations in branching ratios (and hence overall transition probabilities) are also reflected in the measurements of the decay time. As seen in Fig. 5, excitation into the $^5D_1$ state consistently gives higher values for the lifetime of the $^5D_0$ state than are obtained by excitation into the $^5D_2$ state. This is true not only for the line-narrowed emission from equivalent isochromats, but indeed for all manner of excitation, broad band as well as laser, into the respective states. The measured lifetimes are presumably radiative, since the probability of nonradiative deexcitation of the $^5D_0$ state by multiphonon processes is vanishingly small in this host,[22] and their site-dependent behavior parallels reasonably well the relative increase in the proportion of electric dipole emission in the total spectrum.

Thus, it would appear that even before applying line-narrowing techniques, the very choice of pumping transition exerts some degree of selection among the total ensemble of environments, favoring those for which the appropriate optical-transition probability is highest. This preselection has only a minimal effect on the magnitudes of the observed energy-level splittings, determined by the even crystal-field terms, but a much larger one where intensities, governed by the odd terms, are concerned. These effects on the branching ratios are also mirrored by the crystal-field components within a given multiplet, where-

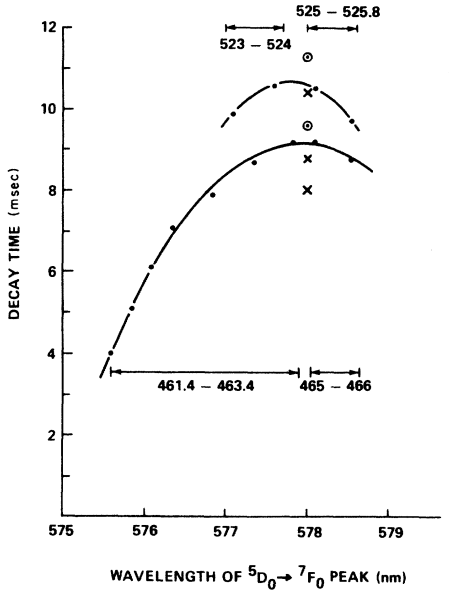


FIG. 5. Decay times of the line-narrowed $^5D_0 \rightarrow {}^7F_0$ fluorescence, as functions of its emission wavelengths. Excitation wavelengths (in nm) are indicated near the corresponding experimental curves. Circled points show the respective long-lifetime limits obtained by measurements in the tail of the decay, while crosses show values obtained under broad-band excitation into (from top) the $^5D_1$, $^5D_2$, and ultraviolet absorptions. Note dependence of decay time upon state initially excited, even for equivalent isochromats (same $^5D_0 \rightarrow {}^7F_0$ wavelength).

in small but significant differences are observed in the intensity patterns of supposedly equivalent isochromats, depending on whether excitation is into the $^5D_1$ or $^5D_2$ state. However, since the energies of the levels themselves are in fact essentially identical, we shall not consider the intensity variations in the subsequent discussion of structure.

One remaining spectral feature worthy of note is the appearance of an unusual amount of non-line-narrowed emission at excitation wavelengths shorter than 463 nm. It is not, of course, unusual for a low-level non-line-narrowed background to underlie the line-narrowed emission, since some untuned broad-band fluorescence from the laser dye does reach the glass sample. The amount of this excitation-independent background was readily measured by simply blocking the feedback from the dye laser grating, and its contribution was found to be generally one and one-half to three orders of magnitude less than the line-narrowed emission. However, at wavelengths shorter than about 463 nm, the decreasing intensity of the line-narrowed emission reveals an anomalously large unnarrowed background. This extraneous emission, which has the same spectral structure as "normal" unnarrowed fluorescence, decreases

in intensity much more slowly with lower-excitation wavelength than does the line-narrowed emission; consequently, its relative contribution rapidly becomes large enough at the shorter-excitation wavelengths to cause substantial distortion of the line-narrowed spectrum, and must be subtracted from the total to reveal the true shape of the latter. At excitations much below 462 nm, the unnarrowed emission has become so large a fraction of the total (more than two-thirds) that subtraction can no longer extract details of the narrowed spectra with any degree of confidence. Nevertheless, the sharp $^5D_0 \rightarrow {}^7F_0$ narrowed emission can still be observed even at excitation wavelengths as short as 460 nm.

The origin of the anomalous non-line-narrowed emission is not clear. More intense than that excited by residual broad-band dye fluorescence, it is apparently pumped by tuned laser excitation since it disappears when feedback from the laser grating is blocked. Its structure is not dependent on excitation wavelength, and its intensity gradually drops to the level of the normal background at excitations below about 455 nm. It is excited only on the short-wavelength side of the absorption into the $^5D_2$ state (and not at all into the $^5D_1$), and at wavelengths where that absorption is so weak and diffuse as to be virtually unmeasurable. This anomalous emission could arise through excitation into an underlying complex of weak vibronic sidebands; such structure is often found in crystalline materials and has recently been observed for the first time in glassy systems.[25] An alternative possibility is that of a site-dependent cross-relaxation process wherein the rate of energy transfer from the high-energy isochromats (characterized by a large crystal field) to their structurally unrelated neighbors is much faster than between the normal sites more typical of the glass. We can offer no definitive explanation with the available information and, considering it not germane to the main intent of this paper, shall not discuss it further.

The energies of the various crystal-field components of the $^7F_1$ and $^7F_2$ states, at each excitation wavelength, are listed in Table I. The splittings themselves are uniquely determined, but there is considerable ambiguity in describing the site dependence of the barycenters of the crystal-field-split levels. In the oxide glass,[11] these had been described with reference to the ground state as constant; however, such description creates the impression that only the $^7F_0$ energy is independent of site, and that the barycenters of all the higher states move sharply upward as the excitation wavelength is decreased, all at just the appropriate rates to enable the emissions to continue to fall in the proper spectral regions. We feel that a physically more meaningful description is obtained if the energies are stated with reference to a higher level, in this case the $^5D_2$, as site independent (similar to Ref. 5). In such a case, we find that the $^5D_0$ state moves only slightly as a function of excitation, and the $^5D_1$ hardly at all. In the lower manifold, the energy of only the $^7F_0$ shows a substantial site-to-site variation, with the zero point taken (arbitrarily) at the wavelength corresponding to the peak of the inhomogeneous absorption envelope; the barycenters of the $^7F_1$ and $^7F_2$ states appear considerably less sensitive to the environment, even while the splittings themselves vary widely. Although the crystal-field treatment (to follow) is concerned only with splittings, this description of the barycenters seems more consonant with the implicit assumptions of the electrostatic field model.

## IV. DISCUSSION

The low symmetry and absence of site-to-site correlation inherent in the glassy state has always made spectral assignment a risky undertaking. Nevertheless, as discussed in an earlier paper,[11] a residue of local order often persists at the site of the emitting ion, in terms of which the gross features of the spectra can be interpreted. In this glass, as before, the most appropriate local symmetry appears to be $C_{2v}$. It is the highest symmetry that allows full splitting of the $^7F_1$ and $^7F_2$ levels of $Eu^{3+}$, allows optical activity for almost all components, and is relatively tractable for crystal-field calculations. This treatment proved successful in previous cases and we shall continue its use here.

Beginning with the $^7F_1$ triplet, we first seek to identify its symmetric, or $M_J = 0$, level. This is nondegenerate in all axial symmetries and does not mix with the others until all symmetry is removed; this fact should be reflected by the spectroscopic behavior of the $^5D_0 \rightarrow {}^7F_1$ emission. In oxide glasses this was manifested in an unusually sharp component, at the lowest emission wavelength of the three, which shifted as a function of pump wavelength much more than any other. In the fluoroberyllate, although no unusually sharp component is found, one of the three emission components does show a massive energy shift, almost 200 $cm^{-1}$ and at least 50% greater than that shown by any other component, and in the opposite direction. Unlike the case in the oxide glasses, this unique $^7F_1$ level is the highest of the three; however, such position interchanges are not uncommon even in closely related crystals (e.g., $YVO_4$ and $YPO_4$),[26] where, because of polarization, the assignments are in-

TABLE I. Site dependence of energy levels of $Eu^{3+}$ in KCaAl fluoroberyllate glass as functions of $^5D_0 \rightarrow {}^7F_0$ wavelength.

| Wavelength of $^5D_0 \rightarrow {}^7F_0$ (nm) | | Energies ($cm^{-1}$)[a,b,c] | | | | | | | | | | |
|---|---|---|---|---|---|---|---|---|---|---|---|---|
| | | $^7F_0$ | $^7F_1$ | | | | $^7F_2$ | | | | $^5D_0$ | $^5D_1$ |
| | | $A_1$ | $B_2$ | $B_1$ | $A_2$ | $A_1$ | $A_2$ | $A_1$ | $B_2$ | $B_1$ | $A_1$ | |
| 578.73 | Meas. | 27.7 | 340.2 | 395.1 | 455.4 | 945.5 | 1022.7 | 1064.7 | 1175.2 | 1216.4 | 17306.9 | 19065.3 |
| | Calc. | | 340.0 | 395.6 | 455.2 | 946.5 | 1022.2 | 1063.7 | 1174.7 | 1217.6 | | |
| 578.53 | Meas. | 18.4 | 326.0 | 388.1 | 456.9 | 939.9 | 1017.4 | 1066.3 | 1162.0 | 1201.9 | 17303.5 | 19064.1 |
| | Calc. | | 324.8 | 390.0 | 456.4 | 943.8 | 1016.1 | 1062.4 | 1159.4 | 1206.2 | | |
| 578.32 | Meas. | 9.2 | 308.8 | 384.2 | 457.8 | 934.1 | 1008.7 | 1062.9 | 1145.1 | 1186.3 | 17300.7 | 19063.2 |
| | Calc. | | 307.9 | 385.4 | 457.7 | 936.6 | 1008.3 | 1060.4 | 1143.0 | 1188.9 | | |
| 578.09 | Meas. | 0 | 289.0 | 378.0 | 463.9 | 928.2 | 977.2 | 1057.9 | 1131.8 | 1175.4 | 17298.2 | 19062.6 |
| | Calc. | | 289.2 | 377.8 | 463.9 | 927.7 | 977.2 | 1058.4 | 1132.3 | 1174.9 | | |
| 577.86 | Meas. | −9.3 | 266.7 | 366.8 | 477.2 | 921.6 | 983.3 | 1053.0 | 1124.7 | 1171.5 | 17296.0 | 19062.5 |
| | Calc. | | 268.6 | 365.3 | 476.9 | 917.6 | 982.5 | 1057.0 | 1129.0 | 1168.2 | | |
| 577.61 | Meas. | −18.7 | 243.9 | 351.0 | 498.0 | 914.6 | 968.6 | 1051.0 | 1125.0 | 1175.6 | 17294.0 | 19062.7 |
| | Calc. | | 247.5 | 348.8 | 497.1 | 907.3 | 966.1 | 1058.3 | 1133.1 | 1170.6 | | |
| 577.36 | Meas. | −28.0 | 221.6 | 332.0 | 524.1 | 906.6 | 954.0 | 1052.6 | 1131.2 | 1186.1 | 17292.2 | 19063.4 |
| | Calc. | | 226.6 | 329.6 | 522.4 | 896.5 | 949.3 | 1062.7 | 1142.5 | 1180.6 | | |
| 577.11 | Meas. | −37.3 | 200.7 | 311.6 | 551.7 | 896.8 | 940.1 | 1057.9 | 1141.0 | 1198.9 | 17290.5 | 19064.5 |
| | Calc. | | 206.4 | 309.5 | 549.3 | 885.1 | 933.5 | 1069.6 | 1154.0 | 1194.1 | | |
| 576.85 | Meas. | −46.7 | 181.8 | 292.2 | 577.3 | 884.7 | 927.2 | 1066.5 | 1152.5 | 1212.1 | 17288.8 | 19066.0 |
| | Calc. | | 187.4 | 290.6 | 574.6 | 873.1 | 919.9 | 1078.1 | 1165.2 | 1208.5 | | |
| 576.59 | Meas. | −56.1 | 165.3 | 275.7 | 597.6 | 869.6 | 915.6 | 1077.2 | 1165.5 | 1224.8 | 17287.1 | 19067.8 |
| | Calc. | | 169.6 | 274.7 | 595.4 | 860.5 | 909.5 | 1086.3 | 1175.3 | 1222.6 | | |
| 576.34 | Meas. | −65.4 | 150.9 | 262.9 | 611.1 | 851.4 | 905.3 | 1088.2 | 1182.4 | 1235.5 | 17285.4 | 19070.0 |
| | Calc. | | 152.5 | 262.6 | 610.2 | 848.0 | 903.0 | 1091.6 | 1186.0 | 1234.8 | | |
| 576.09 | Meas. | −74.8 | 137.0 | 251.1 | 622.5 | 830.5 | 897.1 | 1100.1 | 1196.7 | 1243.7 | 17283.5 | 19072.5 |
| | Calc. | | 135.7 | 251.3 | 623.2 | 833.3 | 899.1 | 1097.3 | 1193.8 | 1244.2 | | |
| 575.85 | Meas. | −84.2 | 123.8 | 241.6 | 629.8 | 807.9 | 890.8 | 1108.2 | 1207.3 | 1249.5 | 17281.5 | 19075.4 |
| | Calc. | | 119.9 | 242.2 | 632.0 | 816.3 | 896.8 | 1099.8 | 1198.5 | 1250.8 | | |
| 575.61 | Meas. | −93.6 | 110.3 | 233.0 | 635.3 | 785.3 | 886.3 | 1110.9 | 1211.8 | 1254.6 | 17279.3 | 19078.6 |
| | Calc. | | 105.0 | 233.8 | 638.3 | 796.8 | 894.5 | 1099.4 | 1199.9 | 1256.3 | | |

[a] Assignments were made in terms of $C_{2v}$ local symmetry and best crystal-field fit for the total ensemble (see text).

[b] To describe the site dependence of the energies, the $^5D_2$ barycenter is assumed constant, independent of site. The zero position of the $^7F_0$ level is taken to correspond to the peak of the inhomogeneously broadened $^5D_0 \rightarrow {}^7F_0$ line and all energies are stated with reference to that.

[c] The quality of the crystal-field fit to the measured energies can be stated by dividing the rms error by the rms Stark splitting. This fractional error ranges between 0.5% and 6.5% with an average of about 4%.

controvertible. We, therefore, take the highest level of the $^7F_1$ as belonging to the symmetric ($A_2$) representation of $C_{2v}$, leaving the other two as $B$ type; since the choice between these is arbitrary, we select the lower as $B_2$.

Greater difficulties are encountered in the $^5D_0 \rightarrow {}^7F_2$ region. Here one emission component (at the lowest wavelength) is generally sharper and stronger than the others, and one (at the highest) is generally weaker. Unlike the case in the oxide glasses, however, no single intensity pattern remains valid throughout the entire range of pump wavelengths, and we can extract no useful assignment information. What saves the situation is the existence of a body of data not available in the oxide case; by pumping into the $^5D_2$ state, it proved possible to obtain line-narrowed spectra not only for emission from the $^5D_0$, but from the $^5D_1$ as well. In terms of radiative mechanism, transitions from the two upper states to the $^7F_{0,1,2}$ are exactly complementary—where one is electric dipole, the other is magnetic—and it is often possible to use the differences in selection rules to identify otherwise ambiguous energy levels. In fact, however, the spectra from the two upper states are remarkably similar: The $^5D_1 \rightarrow {}^7F_1$ transition shows three peaks with the same energy spacing and very nearly the same intensity pattern as is observed for the $^5D_0 \rightarrow {}^7F_1$. Linewidths (in $cm^{-1}$) are essentially the same, and no evidence for multiplet structure is observed, indicating that, as expected at cryogenic temperatures, the bulk of the $^5D_1$ emission originates from the lowest Stark level. Similarities are also observed in the respective $^7F_2$ emissions, with two notable differences: through the entire pump-wavelength range one component (the second) is consistently more intense relative to the others when the emission orig-

inates from the $^5D_1$ state than when it originates from the $^5D_0$, while one other component (the fourth) is consistently weaker (see Fig. 6). This can be explained in terms of the $C_{2v}$ selection rules, which, although not obeyed rigorously, should still be felt in terms of relative effects, as follows.

The $^7F_2$ state belongs to $2A_1+A_2+B_1+B_2$; if the emitting state is $^5D_0$ ($A_1$), the transition is electric dipole in nature, and only that component terminating in the $A_2$ Stark level is formally forbidden in $C_{2v}$ symmetry. With the $^5D_1$ as the upper state, however, the transition is magnetic dipole, and transitions to the $A_2$ Stark level of $^7F_2$ from either the $B_1$ or $B_2$ level of $^5D_1$ become allowed, while a corresponding transition terminating in one of the $B$ Stark levels of $^7F_2$, allowed from the $^5D_0$, becomes forbidden. We have already identified the lowest level of the $^7F_1$ as $B_2$ and would expect the same pattern in the $^5D_1$. By associating the decrease in relative intensity with transitions that become formally forbidden in $C_{2v}$ symmetry, we are led to identify the second and fourth levels of $^7F_2$ as $A_2$ and $B_2$, respectively.

As for the remaining components, no purely spectroscopic clues are available for further identification, and we must apply crystal-field calculations. As discussed in an earlier paper, the crux of the identification process is continuity. Since the individual spectral components can be followed as continuous functions of pump wavelength, we must seek not merely best assignments for each individual spectrum, but a best assignment common to the entire set. Similarly, we must disregard any that require discontinuous changes as the pump wavelength is scanned, or that give substantially better fits at one end of the pump-wavelength range than at the other. With the previously stated identifications, only six nonequivalent assignment sets remain, plus only another six if we allow exchange of the arbitrary choice of $B_1$ and $B_2$ in the $^5D_1$ state. Of these, only one set of assignments even comes close to giving a reasonable fit for the entire pump-wavelength range. This set, with its full range of site-dependent values, is given in Table I and Fig. 7, and the pertinent crystal-field parameters are given in Table II and Fig. 8.

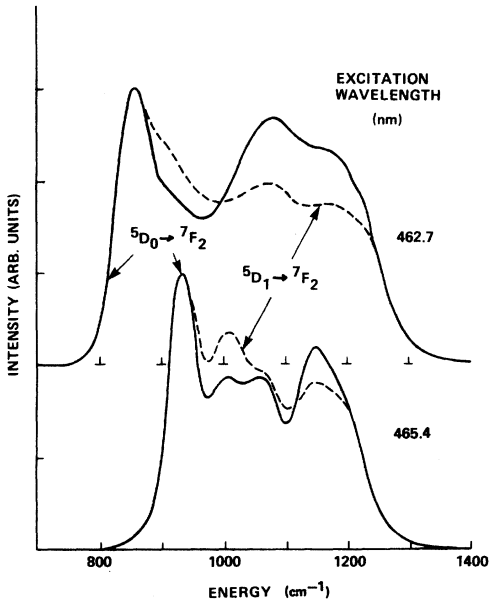


FIG. 6. Fluorescence emission from corresponding transitions terminating in the $^7F_2$ state, at two excitation wavelengths. Solid lines show the emission from the $^5D_0$ state; broken lines, from the $^5D_1$. Abscissa scale refers to energy difference from emitting state, and all intensities are normalized with regard to the most intense peak. The second component of the emission (from left) is consistently more intense when originating from the $^5D_1$ state, while the fourth is consistently weaker. The third is erratic and shows no consistent intensity pattern.

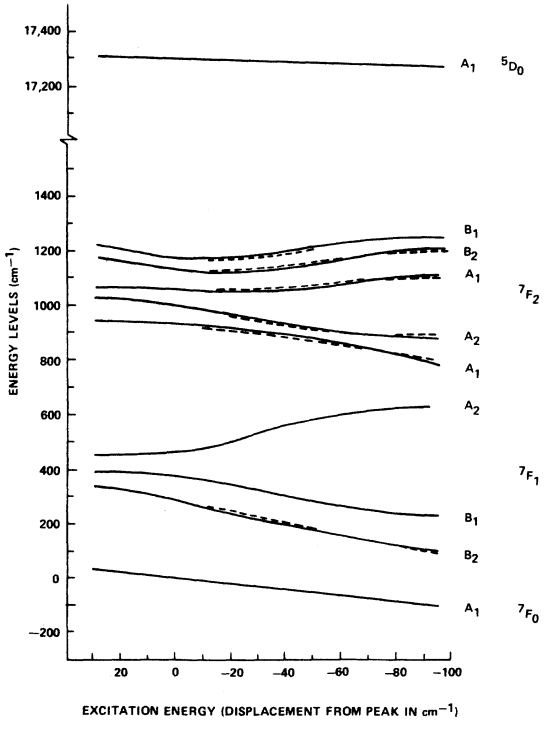


FIG. 7. Excitation dependence of the Stark components of the energy levels of $Eu^{3+}$ in KCaAl fluoroberyllate glass (at 80 K). Assignments were made on the basis of $C_{2v}$ local symmetry and best fit to electrostatic crystal-field calculations (see text). The solid lines show the measured values; broken lines, calculated values for best fit.

TABLE II. Site dependence of crystal-field parameters for $Eu^{3+}$ in KCaAl fluoroberyllate glass as functions of $^5D_0 \rightarrow {}^7F_0$ wavelength.

| Wavelength of $^5D_0 \rightarrow {}^7F_0$ (nm) | | Barycenters ($cm^{-1}$) $^7F_1$ | $^7F_2$ | Crystal-field parameters ($cm^{-1}$)[a,b] $B_{20}$ | $B_{22}$ | $B_{40}$ | $B_{42}$ | $B_{44}$ | Ratios $B_{22}/B_{20}$ | $B_{42}/B_{40}$ | $B_{44}/B_{40}$ |
|---|---|---|---|---|---|---|---|---|---|---|---|
| 578.73 | Meas. | 396.9 | 1084.9 | 145.7 | −139.1 | 188.9 | −283.4 | −65.0 | −0.955 | −1.501 | −0.344 |
| | Calc. | | | 184.3 | −163.6 | 125.3 | −203.0 | −53.7 | −0.888 | −1.619 | −0.428 |
| 578.53 | Meas. | 390.4 | 1077.6 | 165.0 | −162.9 | 173.1 | −318.8 | −39.0 | −0.987 | −1.841 | −0.225 |
| | Calc. | | | 206.3 | −190.2 | 121.8 | −233.8 | −32.5 | −0.922 | −1.919 | −0.267 |
| 578.32 | Meas. | 383.6 | 1067.4 | 185.1 | −193.8 | 155.8 | −340.9 | −4.6 | −1.047 | −2.189 | −0.029 |
| | Calc. | | | 226.5 | −223.1 | 116.9 | −260.0 | −3.9 | −0.985 | −2.223 | −0.033 |
| 578.09 | Meas. | 377.0 | 1058.1 | 217.3 | −221.4 | 143.2 | −350.5 | 22.1 | −1.019 | −2.448 | 0.154 |
| | Calc. | | | 253.1 | −246.3 | 117.0 | −287.2 | 19.5 | −0.973 | −2.455 | 0.167 |
| 577.86 | Meas. | 370.3 | 1050.9 | 266.6 | −241.8 | 137.4 | −353.6 | 39.2 | −0.907 | −2.574 | 0.286 |
| | Calc. | | | 289.6 | −256.2 | 123.4 | −317.9 | 36.6 | −0.885 | −2.575 | 0.297 |
| 577.61 | Meas. | 364.5 | 1047.1 | 331.6 | −253.3 | 137.9 | −356.4 | 47.3 | −0.764 | −2.585 | 0.343 |
| | Calc. | | | 335.6 | −255.4 | 135.8 | −351.0 | 46.8 | −0.761 | −2.585 | 0.345 |
| 577.36 | Meas. | 359.5 | 1046.3 | 407.1 | −257.5 | 142.9 | −362.5 | 50.5 | −0.633 | −2.536 | 0.353 |
| | Calc. | | | 388.9 | −249.5 | 152.0 | −384.3 | 52.4 | −0.642 | −2.529 | 0.345 |
| 577.11 | Meas. | 355.1 | 1047.3 | 485.5 | −257.7 | 149.5 | −370.6 | 54.8 | −0.531 | −2.479 | 0.366 |
| | Calc. | | | 444.4 | −242.5 | 168.7 | −414.7 | 59.0 | −0.546 | −2.458 | 0.350 |
| 576.85 | Meas. | 350.9 | 1049.0 | 559.3 | −258.1 | 156.1 | −383.7 | 62.5 | −0.461 | −2.457 | 0.400 |
| | Calc. | | | 498.2 | −238.4 | 183.3 | −444.0 | 69.0 | −0.479 | −2.422 | 0.376 |
| 576.59 | Meas. | 346.6 | 1050.8 | 622.0 | −262.8 | 163.3 | −403.2 | 76.9 | −0.423 | −2.470 | 0.471 |
| | Calc. | | | 547.9 | −241.0 | 194.5 | −472.4 | 85.6 | −0.440 | −2.429 | 0.440 |
| 576.34 | Meas. | 341.8 | 1052.7 | 671.2 | −275.2 | 172.1 | −419.1 | 100.6 | −0.410 | −2.435 | 0.585 |
| | Calc. | | | 591.3 | −252.4 | 204.9 | −489.4 | 112.1 | −0.427 | −2.389 | 0.547 |
| 576.09 | Meas. | 336.7 | 1053.3 | 716.2 | −289.0 | 178.0 | −437.0 | 143.3 | −0.404 | −2.455 | 0.805 |
| | Calc. | | | 632.0 | −265.3 | 210.4 | −506.9 | 159.3 | −0.420 | −2.409 | 0.757 |
| 575.85 | Meas. | 331.4 | 1052.4 | 751.5 | −305.6 | 184.1 | −458.1 | 198.2 | −0.407 | −2.489 | 1.077 |
| | Calc. | | | 669.6 | −282.4 | 213.4 | −522.7 | 218.5 | −0.422 | −2.450 | 1.024 |
| 575.61 | Meas. | 325.7 | 1049.4 | 781.5 | −321.8 | 190.7 | −487.8 | 260.2 | −0.412 | −2.558 | 1.365 |
| | Calc. | | | 708.6 | −300.9 | 214.8 | −543.5 | 282.6 | −0.425 | −2.530 | 1.315 |

[a] "Measured" values are those obtained from the crystal-field fit to the observed energies (see Table I); "calculated" values are derived from the structural model. In the latter case, the values were extracted in the form of dimensionless Tesseral harmonics, which are related to the physical parameters by two multiplicative factors, one for each order. These factors were assumed to be constant over the full range of measurement, and were derived empirically by a best logarithmic fit to the complete data set.

[b] Quality of fit for the calculated values, in terms of percent deviation, varies from 28% at the low-field (long wavelength) end of the range of $^5D_0 \rightarrow {}^7F_0$ wavelengths, to 10% at the other end, and averages about 15%. The ratios, which are independent of the multiplicative factors, show a much better fit, 11% and 3% at the respective ends of the measurement range, with an average of about 5%.

To understand the structural implications of these results, we must generate a geometric model of the arrangement of ligands surrounding the emitting ion. As in the previous works on oxide glasses,[11,12] we limit our consideration to the immediate environment of the $Eu^{3+}$ ion, and simulate it with a simple array of point changes of the appropriate symmetry, whose electrostatic field will reproduce the behavior of the ratios of the measured parameters. The reasons for concentrating on structures involving eightfold or ninefold coordination were also discussed: appropriate ionic size and available bonding orbitals, the ubiquitousness of eightfold and ninefold coordination in crystalline rare-earth compounds, and the absence of chemical or structural constraints that might prevent the rare earth from achieving its maximum coordination. Since this is no less true in the fluoride case than in the oxide, we will follow the same procedure here.

Having previously developed a suitable structural model for the coordination in oxide glasses, we should first examine this model for its applicability to the fluoroberyllate glass system. This model involves eight coordinators essentially equidistant from the $Eu^{3+}$ ion, arranged in a distorted antiprism with $C_{2v}$ symmetry, and a ninth coordinator along the $C_2$ axis at a variable distance from the central ion. The model does, in fact, give reasonable agreement to the observed changes in magnitude: $B_{20}$ increases by a factor of 5, $B_{40}$ changes relatively little, and $B_{44}$ increases sharply and changes sign. In every case, however, these geometrically derived parameters have the

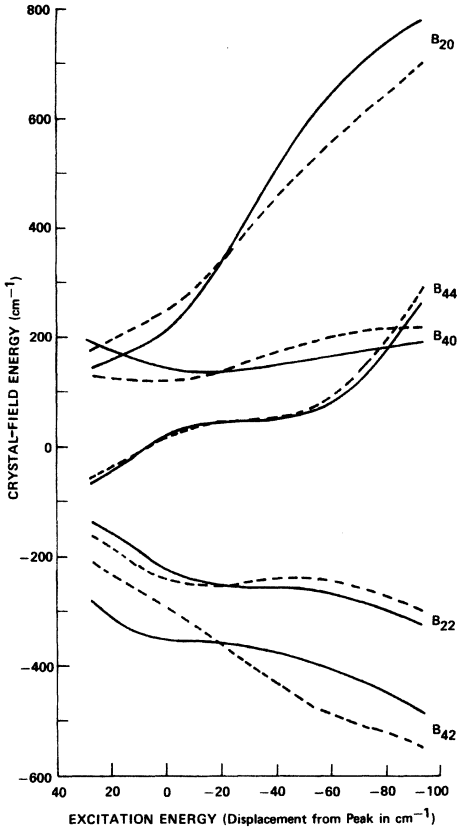


FIG. 8. Excitation dependence of the second-order and fourth-order crystal-field parameters for $Eu^{3+}$ in KCaAl fluoroberyllate glass (at 80 K). Calculations were made on the basis of assignments shown in Fig. 7. Solid lines show values extracted directly from spectroscopic data; broken lines, values derived from geometric model. In the latter case, the second-order and fourth order proportionality constants relating geometric to spectroscopic values were obtained empirically.

opposite sign from what is observed. While the signs are essentially arbitrary for the $B_{22}$ and $B_{42}$ terms (depending only on the naming of the $x$ and $y$ axes), the other three are uniquely determined by the spectral assignments and must be satisfied. It was, in fact, quite feasible to satisfy the requirements of sign and magnitude for any of the crystal-field parameters by suitable variations in the geometric parameters of the structural model. What proved impossible to do, however, was to satisfy the signs and magnitudes of all of them, plus their relative changes as functions of distortion (caused by the ninth coordinator), and still maintain the packing density and $C_{2v}$ symmetry of the eight equidistant primary coordinators. Moreover, structures with seven or fewer primary coordinators gave even less satisfactory results, while larger numbers of primary coordinators required an intolerably large radial distance to the central coordinating ion.

Seeking a suitable structural model, we considered the various kinds of structural modifications possible within the context of close-packed eightfold or ninefold coordination having $C_{2v}$ symmetry. This analysis revealed that with only a small alteration in our starting assumptions, a structural model can be generated that would exhibit appropriate behavior in both sign and magnitude for all five crystal-field parameters. This change involves the segregation of the primary coordinators into two different classes based on radial distance. The resultant new model is a ninefold coordinated structure, with three of the coordinators (designated "peri-") lying some 5% closer to the central ion than do the other six ("apo-"). As shown in Fig. 9, the arrangement can be best described by starting with a trigonal face-centered prism (on the left), then stretching its upper and lower triangular surfaces to isosceles and inclining them with their apices closer than their bases. The three equatorial points locating the peri-coordinators also lie in an isosceles triangle, this one somewhat compressed along the $C_2$ axis. The structure thereby obtained (on the right) retains some resemblance to the capped antiprism model appropriate for oxide glasses, but with considerable elongation in the $y$ direction (perpendicular to the $C_2$ axis). The parametric variation corresponding to the range of pump energies would be reflected in the difference between the average distances of the two coordinator classes, with the higher crystal field associated with the larger radial difference and hence the closer approach of the peri-coordinators. The crystal-field parameters calculated with this model agree with the spectroscopic values generally within 20%, a figure that we consider quite respectable.[27]

As in the case of the oxide glasses, we can offer no independent support for this hypothetical model. The differences can be attributed to the chemical differences between oxygen and fluorine themselves. The degree of covalency in the metal-oxygen bond should be considerably more than in the metal-fluorine bond; indeed, the fluoroberyllate network is considered to be almost totally ionic in nature.[28] Furthermore, to whatever extent covalency enters the picture in the fluorine case, the much greater electronegativity of the latter and its univalent bonding should tend toward much greater bridging asymmetry than in the oxide case. Thus the model can be viewed as an $EuF_3$ entity that has become solvated by $BeF_2$ groups through the formation of nine slightly asymmetric fluorine bridges. Again, as in the oxide case, we have a model that is chemically consistent

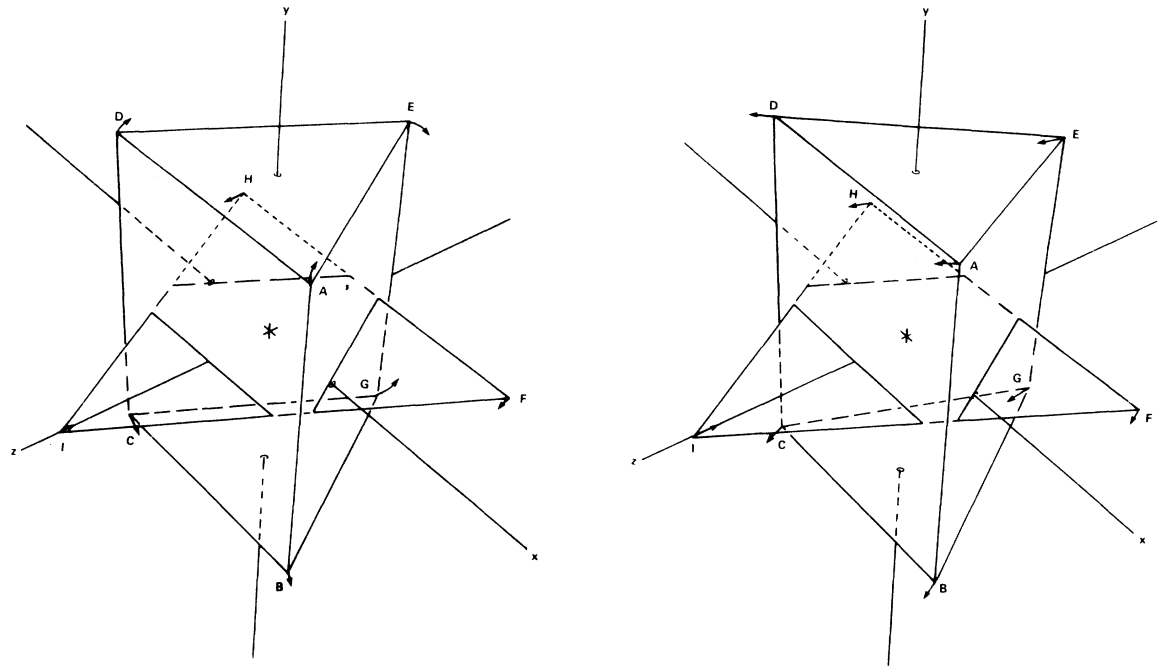


FIG. 9. Geometry of the coordination model. In the trigonal face-centered prism (left), faces ADE and BCG are equilateral triangles perpendicular to the $y$ axis, while vertices FHI form another equilateral triangle in the $xz$ plane. The Cartesian axes are shown where they emerge from the trigonal prism. The arrows at the vertices show the distortions required to reach the "low-field model" for the coordination structure (right); these directions cause faces ADE and BCG to become elongated in the $z$ direction and inclined so that prism edge EG is shorter than edges AB and CD, destroying all symmetry elements except rotation about the $z$ axis and reflection across the $xz$ and $yz$ planes. Triangle FHI has become deformed into isosceles by compression in the $z$ direction, which remains the $C_2$ axis. This model depicts the structure at the long-wavelength (low-crystal-field) end of the measurements, and the arrows show the distortion directions from this structure for stronger fields. In this process, the radial distances from the origin to points EGI decrease, while radial distances to the others increase. The model is consistent with minimum fluorine-fluorine and curopium-fluorine distances of about 2.4 and 2.8 Å, respectively; the average difference between radial distances from $Eu^{3+}$ to the peri- and apo-coordinators ranges from 5–6%, while the average differences within the two groups ranges from 1–4%.

and is the least complicated arrangement that can give reasonable agreement to the spectroscopically derived parameters.

## V. CONCLUSION

The foregoing treatment should not, of course, be viewed out of its proper context. Despite the acknowledged limitations of the electrostatic crystal-field approach, no greater sophistication is warranted. The site-selection process is far from complete, and the large inhomogeneous widths that remain in the spectra of individual isochromats may cloak a wide range of unknown and unmeasurable variations. Thus, the excitation-dependent pattern of the Stark splittings, and the structural model proposed as a physical rationalization, reflect only an unspecified average behavior for the corresponding sites.

Nevertheless, this work has revealed that the demonstrated similarities in the spectroscopic behavior of $Eu^{3+}$ in a wide variety of oxidic glasses is not directly carried over into their fluoridic analogs. Although significant differences are observable even under broad-band excitation, only with fluorescence line-narrowing measurements can the extent of the differences—the site-dependent spectral behavior, the assignments, and the structural model—be fully appreciated. Yet, two major parallels remain: In all glasses thus far studied, the spectra are consistent with variants of ninefold coordination in the immediate environment of the $Eu^{3+}$ ion; and, more importantly, isochromats whose $^5D_0 \rightarrow {}^7F_0$ energies lie toward the high end of the total range are invariably associated with greater Stark splittings, shorter decay times, and greater structural distortion of the site. The situation in other glasses, particularly with mixed anions,[15,29] remains to be seen.

## ACKNOWLEDGMENTS

This work was supported, in part, by Lawrence Livermore Laboratory, under U. S. Department

of Energy Contract No. W7405-ENG-48, which we gratefully acknowledge. We also thank B. W. Hawkins and J. Walsh for recording many of the line-narrowed spectra, C. M. Baldwin of UCLA for producing the glass samples, and J. R. McColl for helpful discussions. We wish to express particular appreciation to M. J. Weber for his continuous interest. His numerous comments and suggestions helped immeasurably in the completion of this work.

[1]A. Szabo, Phys. Rev. Lett. 25, 924 (1970); 27, 323 (1971).

[2]L. A. Riseberg, Phys. Rev. Lett. 28, 789 (1972); Solid State Commun. 11, 469 (1972); Phys. Rev. A 7, 671 (1973).

[3]N. Motegi and S. Shionoya, J. Lumin. 8, 1 (1973).

[4]P. Avouris, A. Campion, and M. A. El-Sayed, Chem. Phys. Lett. 50, 9 (1977); J. Chem. Phys. 67, 3397 (1977).

[5]T. Kushida and E. Takushi, Phys. Rev. B 12, 824 (1975); E. Takushi and T. Kushida, J. Lumin. 18/19, 661 (1979).

[6]P. M. Selzer, D. L. Huber, D. S. Hamilton, W. M. Yen, and M. J. Weber, Phys. Rev. Lett. 36, 813 (1976); also in *Structure and Excitation of Amorphous Solids*—1976, proceedings of the 1976 Williamsburg Meeting of the Division of Structure and Excitation of Amorphous Solids of the American Physical Society, edited by G. Lucovsky and F. L. Galeener (A.I.P., New York, 1976), p. 328.

[7]C. Brecher, L. A. Riseberg, and M. J. Weber, Appl. Phys. Lett. 30, 475 (1977).

[8]M. J. Weber, *Proceedings of the Seventh International Conference on Amorphous and Liquid Semiconductors*, edited by W.E. Spear (University of Edinburgh, Edinburgh, 1977), p. 645.

[9]C. Brecher, L. A. Riseberg, and M. J. Weber, Phys. Rev. B 18, 5799 (1978).

[10]C. Brecher, L. A. Riseberg, and M. J. Weber, J. Lumin. 18/19, 651 (1979).

[11]C. Brecher and L. A. Riseberg, Phys. Rev. B 13, 81 (1976).

[12]C. Brecher, L. A. Riseberg, and M. J. Weber, in *Proceedings of the Twelfth Rare Earth Research Conference*, edited by C. E. Lundin (University of Denver, Denver, 1976), Vol. I, p. 351.

[13]M. J. Weber, J. Hegarty, and D. H. Blackburn, in *Borate Glasses: Structure, Properties, Materials Science Research, Vol.* 12, edited by L. D. Pye, V. D. Frechette, and N. J. Kreidl (Plenum, New York, 1978), p. 215.

[14]J. Hegarty, W. M. Yen, M. J. Weber, and D. H. Blackburn, J. Lumin. 18/19, 657 (1979).

[15]C. Brecher and L. A. Riseberg, Conference on Electrical Magnetic, and Optical Properties of Glasses, Troy, New York, 1979, J. Non-Cryst. Solids (to be published).

[16]Reviewed by K. H. Sun, 80th Annual Meeting of the American Ceramic Society, Detroit, Michigan, 1978 (unpublished).

[17]M. Poulain, M. Poulain, and J. Lucas, Mater. Res. Bull. 10, 243 (1975); M. Poulain, M. Chanthanasinh, and J. Lucas, *ibid.* 12, 151 (1977); M. Matecki, M. Poulain, M. Poulain, and J. Lucas, *ibid.* 13, 1039 (1978).

[18]J. Lucas, M. Chanthanasinh, M. Poulain, M. Poulain, P. Brun, and M. J. Weber, J. Non-cryst. Solids 27, 273 (1978); J. Lucas and M. Poulain, *The Rare Earths in Modern Science and Technology*, proceedings of the 13th Rare Earth Research Conference, edited by G. McCarthy and J. J. Rhyne (Plenum, New York, 1978), p. 259.

[19]M. W. Shafer, P. B. Perry, and I. F. Chang, Spring Meeting of the Electrochemical Society, 1978, Seattle, Washington, Extended Abstracts, p. 854 (unpublished).

[20]Coined by M. J. Weber and W. M. Yen.

[21]J. Hegarty, W. M. Yen, and M. J. Weber, Phys. Rev. B 18, 5816 (1979); see also, Ref. 13 and 14.

[22]L. A. Riseberg and J. J. Weber, *Progress in Optics*, edited by E. Wolf (North-Holland, Amsterdam, 1978), Vol. 14, and Refs. cited therein; see also C. Layne and M. J. Weber, Phys. Rev. B 16, 3259 (1977).

[23]As, for example, in $Cs_2NaEuCl_6$; see O. A. Serra and L. C. Thompson, Inorg. Chem. 15, 504 (1976).

[24]See, for example, S. Hufner, *Optical Spectroscopy of Transparent Rare-Earth Compounds* (Academic, New York, 1978), p. 106; G. J. Linford, R. A. Saroyan, J. B. Trenholme, and M. J. Weber, IEEE J. Quantum Electron. QE15, 510 (1979); R. D. Peacock, J. Mol. Struct. 46, 203 (1978).

[25]V. K. Zakharov, I. V. Kovaleva, V. P. Kolobkov, and L. F. Nikolaev, Opt. Spektrosk. 42, 926 (1977) [Opt. Spectrosc. (USSR) 42, 532 (1977)] For direct measurements on vibrational modes in $BeF_2$ glass, see F. L. Galeener, G. Lucovsky, and R. H. Geils, Solid State Commun 25, 405 (1978).

[26]C. Brecher, H. Samelson, A. Lempicki, R. Riley, and T. Peters, Phys. Rev. 155, 178 (1967); C. Brecher, H. Samelson, R. Riley, and A. Lempicki, J. Chem. Phys. 49, 3303 (1968).

[27]It is interesting that the sites with the greatest distortion also show the greatest relative intensity of electric dipole transitions (particularly the $^5D_0 \rightarrow {}^7F_0$), consistent with Ofelt's theory; see G. S. Ofelt, J. Chem. Phys. 37, 511 (1962). The effect of structural distortion on hypersensitive transitions is also treated by Peacock (Ref. 24).

[28]Pauling estimates the Be-F bond to be 79% ionic in nature; see L. Pauling, *The Nature of the Chemical Bond*, 3rd ed. (Cornell University, Ithaca, 1960), p. 102.

[29]C. Brecher (unpublished).